Turbo Codes for APD-Detected PPM*

Jon Hamkins and Meera Srinivasan

Jet Propulsion Laboratory
California Institute of Technology
4800 Oak Grove Drive
Pasadena, CA 91109-8099
{hamkins,meera.srinivasan}@jpl.nasa.gov

Abstract

This paper introduces a method to use binary turbo codes with high order pulse position modulation (PPM) and an avalanche photodiode (APD) detector typical of an optical communications system. In general, the turbo codes outperform the Reed-Solomon codes usually recommended for this application. The simulation results are obtained from an accurate modeling of the APD output statistics, instead of Gaussian approximations which are often used but which also can over-predict or under-predict symbol error probabilities.

1 Introduction

Optical communication systems currently under development for the deep space channel use high order pulse position modulation (PPM) as the data modulation format. Information bits are encoded, modulated using M-ary PPM, transmitted optically, and received by an avalanche photodiode (APD) detector. For each PPM symbol, the APD produces M soft outputs corresponding to the output electron count for each slot duration.

The exact distribution of output electrons from the APD has been given in [4, 8], but is cumbersome to use, and may be approximated very closely by the Webb density function [13]. In addition, the follow-on electronics contribute additive Gaussian thermal noise to the APD shot noise. A simpler analysis involves modeling both APD shot noise and Gaussian thermal noise as a single Gaussian process. In [5], it was shown that for 4-ary PPM, the purely Gaussian approximation overestimates PPM symbol error probability in the region $P_e < 0.01$. In this paper we provide symbol error probability calculations using both the accurate Webb plus Gaussian model as well as the strictly Gaussian approximation for 256-ary PPM, and show that the Gaussian approximation may either over-predict or under-predict symbol error probability by varying degrees depending upon the levels of background and signal light levels. An upper bound using the Webb plus Gaussian mixture density is provided as a more uniform method of estimating PPM symbol error probability.

Using the Webb model of APD shot noise, we can accurately simulate the performance of a coded system. We introduce a binary turbo coding scheme for high order PPM, and compare it to equivalent rate Reed-Solomon codes. Previous work on coded PPM signaling (see, e.g., [9]) has concentrated on Reed-Solomon codes because their alphabet sizes are easily matched to

*The research described in this paper was carried out at the Jet Propulsion Laboratory, California Institute of Technology, under a contract with the National Aeronautics and Space Administration.

the PPM order, resulting in a one-to-one correspondence between code symbols and PPM symbols. Since every Reed-Solomon code is a maximum distance code, it might seem that no more powerful code could be found for this application.

However, a disadvantage of a Reed-Solomon code is that the decoder does not use the soft detector outputs directly, but instead operates on decoded PPM symbols and erasures. This is an inherent limitation of Reed-Solomon codes, because there is no method to modify Reed-Solomon codes to make full use of the soft information. We thus have the motivation for using turbo codes, which are already known to have outstanding performance in other applications and can operate on the soft counts directly rather than having to use explicit PPM symbol decisions.

This paper makes three new contributions: (1) Uncoded PPM symbol error probability calculations for 256-ary PPM, (2) A binary turbo coding scheme for high order PPM that fully utilizes soft information, and (3) A simulation of end-to-end BER performance for baseline Reed-Solomon codes and binary turbo codes using an accurate statistical model of the APD detector in the absence of thermal noise.

2 APD Receiver Modeling

The average number of photons absorbed by an APD illuminated with total optical power $P(t)$ in T_s seconds can be expressed as

$$\bar{n} = \frac{\eta}{h\nu}\int_0^{T_s} P(t)dt \tag{1}$$

where h is Planck's constant, ν is the optical frequency, and η is the detector's quantum efficiency, defined as the ratio of absorbed to incident photons. The actual number of photons absorbed, n, is a Poisson distributed random variable with rate $\bar{n}$. The conditional probability that an APD generates m electrons in response to exactly n absorbed photons, $m \geq n$, $n > 0$, has been shown by McIntyre to be [8]

$$p(m|n) = \frac{n\Gamma\left(\frac{m}{1-k}+1\right)}{m(m-n)!\Gamma\left(\frac{km}{1-k}+n+1\right)}\left[\frac{1+k(G-1)}{G}\right]^{n+km/(1-k)}\left[\frac{(1-k)(G-1)}{G}\right]^{m-n} \tag{2}$$

where G is the average APD gain, and k is the ionization ratio. Averaging over the exact number of absorbed photons, we obtain

$$p(m|\bar{n}) = \sum_{n=1}^{m} p(m|n)\frac{\bar{n}^n}{n!}e^{-\bar{n}}, \qquad m \geq 1 \tag{3}$$

as the distribution of APD output electrons generated over T_s seconds given the mean number of absorbed photons in that interval. If no photons are absorbed, then no electrons can be generated according to this model. Conversely, no electrons are generated only if no photons have been absorbed. Hence, $p(m=0|\bar{n}) = p(n=0|\bar{n}) = e^{-\bar{n}}$.

An approximation to Equation (3) has been derived by Webb [13] and provides a much simpler expression for the density of m in response to the mean number of photons absorbed:

$$p_w(m|\bar{n}) = \frac{1}{\sqrt{2\pi\bar{n}G^2F}\left(1+\frac{m-G\bar{n}}{\bar{n}GF/(F-1)}\right)^{3/2}}\exp\left(-\frac{(m-G\bar{n})^2}{2\bar{n}G^2F\left(1+\frac{m-G\bar{n}}{\bar{n}GF/(F-1)}\right)}\right) \tag{4}$$

where $F = kG + (2 - 1/G)(1-k)$. This density is a continuous function that is defined for $m > -\lambda G/(F-1)$, and integrates to one in that range. The discrete probabilities in (3) are approximated by evaluating (4) at integer values of m. Note that (4) is defined for negative values of m, provided $m > -\lambda G/(F-1)$, even though negative m has no physical meaning. In the numerical evaluations presented here, we calculate the sum of the Webb density values for $m \geq 1$, and assign to $p(m=0|\bar{n})$ the value of this sum subtracted from one.

Added to the random number of APD output electrons is an independent Gaussian thermal noise charge from the follow-on electronics. The total charge is then integrated over each slot time T_s, resulting in a vector of M independent observables for each received PPM word. It was proven in [12] that given these observables, the maximum likelihood detector structure consists of choosing the PPM symbol corresponding to the slot with the maximum accumulated charge value. If $\bar{n}_b$ and $\bar{n}_s$ are the mean number of absorbed background photons per slot and the mean number of absorbed signal photons per pulse, respectively, the M-ary PPM symbol error probability is

$$P_e(M) = 1 - \int_{-\infty}^{\infty} p(x|\bar{n}_b + \bar{n}_s) \left[\int_{-\infty}^{x} p(y|\bar{n}_b) dy \right]^{M-1} dx, \tag{5}$$

where $p(x|\bar{n})$ is the probability density function for the slot statistic given $\bar{n}$ mean number of absorbed photons over the slot duration. Since the slot statistic is a random variable consisting of the sum of independent Webb and Gaussian random variables, its density function is the convolution of the individual densities, and may be written as

$$p(x|\bar{n}) = \sum_{m=0}^{\infty} \phi(x, \mu_m, \sigma^2) p_w(m|\bar{n}), \tag{6}$$

where $\phi(x, \mu_m, \sigma^2)$ is the Gaussian density function with mean $\mu_m = mq + I_s T_s$ and variance $\sigma^2 = \left(2qI_s + \frac{4\kappa T}{R}\right) BT_s^2$, as given in [5]. Here, q is the electron charge, κ is Boltzmann's constant, T is the equivalent noise temperature, B is the single-sided noise bandwidth, and I_s is the APD surface leakage current. Note that the APD surface leakage current is not multiplied by the APD gain and is modeled here as a constant DC current. The APD dark current, on the other hand, is multiplied by the APD gain and is modeled as part of the background radiation, i.e., it is incorporated into the value of $\bar{n}_b$.

An approach that is sometimes used to simplify calculation of PPM symbol error probabilities is to model the density of the APD output electron charge as Gaussian with mean $qG\bar{n}$ and variance $q^2G^2F\bar{n}$. Then the slot statistic consisting of the sum of APD output electrons and amplifier thermal noise is also Gaussian, and has mean $\mu = qG\bar{n} + I_s T_s$ and variance $\sigma^2 = \left[2q^2G^2F\bar{n} + qI_sT_s + \frac{4\kappa T T_s}{R}\right] BT_s$. Although simple, this approximation does not yield accurate results over all regions of interest, as previously shown in [5] for 4-PPM and as we demonstrate here for 256-PPM.

3 Uncoded PPM Symbol Error Probabilities

Substituting (6) into (5), the PPM symbol error probability may be expressed as

$$\begin{aligned} P_e(M) &= 1 - \int_{-\infty}^{\infty} \sum_{m=0}^{\infty} \phi(x, \mu_m, \sigma^2) p_w(m|\bar{n}_b + \bar{n}_s) \left[\int_{-\infty}^{x} \sum_{n=0}^{\infty} \phi(y, \mu_n, \sigma^2) p_w(n|\bar{n}_b) dy \right]^{M-1} dx \\ &= \sum_{m=0}^{\infty} p_w(m|\bar{n}_b + \bar{n}_s) \int_{-\infty}^{\infty} \phi(x, \mu_m, \sigma^2) \left(1 - \left[\sum_{n=0}^{\infty} p_w(n|\bar{n}_b) \Phi\left(\frac{x - \mu_n}{\sigma}\right) \right]^{M-1} \right) dx, \end{aligned} \tag{7}$$

where $\Phi(x)$ is the Gaussian distribution function $\Phi(x) = \int_{-\infty}^{x} \frac{1}{\sqrt{2\pi}} e^{-u^2/2} du$. The expression in (7) is difficult and time-consuming to evaluate accurately, so an upper bound is calculated instead. Although the union bound is commonly used for such M-ary orthogonal signaling problems, a tighter bound was derived by Hughes [7] and is applied here. By observing that the function $f(u) = 1-[1-u]^{M-1}$ is concave for $u \in [0,1]$, Jensens's inequality gives us $E[f(u)] \leq f(E[u])$. Letting $u = \int_x^{\infty} p(y|\bar{n}_b)dy$ and taking the expectation over x with density function $p(x|\bar{n}_b + \bar{n}_s)$, we can then show that

$$\begin{aligned} P_e(M) &= \int_{-\infty}^{\infty} p(x|\bar{n}_b + \bar{n}_s) \left(1 - \left[1 - \int_x^{\infty} p(y|\bar{n}_b)dy\right]^{M-1}\right) dx \\ &\leq 1 - \left[1 - \int_{-\infty}^{\infty} p(x|\bar{n}_b + \bar{n}_s) \int_x^{\infty} p(y|\bar{n}_b)dydx\right]^{M-1}. \end{aligned} \tag{8}$$

The double integral within the brackets on the right hand side of (8) is simply the probability that a given background slot has a greater electron count than the signal plus background slot. This may also be interpreted as the symbol error probability for equiprobable binary PPM signaling, denoted as $P_e(2)$, and given by

$$P_e(2) = \sum_{m=0}^{\infty} p_w(m|\bar{n}_b + \bar{n}_s) \int_{-\infty}^{\infty} \phi(x, \mu_m, \sigma^2) \sum_{n=0}^{\infty} p_w(n|\bar{n}_b) \Phi\left(-\frac{x-\mu_n}{\sigma}\right) dx, \tag{9}$$

so that the upper bound on the M-ary PPM symbol error probability may now be expressed as $P_e(M) \leq 1 - (1 - P_e(2))^{M-1}$.

Although the upper bound in (8) may be calculated relatively easily, it does require repeated evaluation of the Webb density and nested summation and integration. Use of the Gaussian approximation to the APD statistics saves computational time. Using this Gaussian approximation, the M-ary PPM symbol error probability is given by

$$P_{e,\text{Gaussian}}(M) = \int_{-\infty}^{\infty} \phi(x, \mu_s, \sigma_s^2) \left[1 - \Phi\left(\frac{x-\mu_b}{\sigma_b}\right)^{M-1}\right] dx, \tag{10}$$

where $\mu_b = qG\bar{n}_b + I_s T_s$, $\mu_s = qG(\bar{n}_b + \bar{n}_s) + I_s T_s$, $\sigma_b^2 = \left[2q^2G^2F\bar{n}_b + qI_sT_s + \frac{4\kappa T T_s}{R}\right] BT_s$, and $\sigma_s^2 = \left[2q^2G^2F(\bar{n}_b + \bar{n}_s) + qI_sT_s + \frac{4\kappa T T_s}{R}\right] BT_s$ [5].

The two expressions for evaluating PPM symbol error probability given in equations (8) and (10) were calculated and compared using the following parameters: $M = 256$, $T_s = 2 \times 10^{-8}$ seconds, $k = 0.007$, $I_s = 2 \times 10^{-9}$ amps, $T = 300°$ K, $R = 146650\Omega$, and $B = 1/2T_s = 2.5 \times 10^7$ Hz ($1/2T_s$ is the noise equivalent bandwidth for an ideal integrator over duration T_s). Calculations were performed for several different values of $\bar{n}_b$ and $\bar{n}_s$. The APD gain parameter G was optimized for each pair $\{\bar{n}_b, \bar{n}_s\}$ by taking on the value resulting in minimum PPM symbol error probability. The optimization was performed separately for the Webb and the Gaussian models, resulting in different optimum gains for each model. In addition to numerical evaluation, Monte Carlo simulations of the receiver performance under the Webb model were performed in order to obtain more accurate results for lower SNR regions than those provided by the upper bound (8). In the Monte Carlo simulations, the Webb deviates needed to simulate APD output were generated using the inclusion-exclusion principle [10] following the method outlined in [11].

Fig.s 1-2 show plots of P_e versus $\bar{n}_s$ for three particular values $\bar{n}_b$: 0.01, 1.0, and 100.0. The three curves shown are the error probability for the Webb model obtained through Monte Carlo

simulation, the upper bound for the Webb model as given by (8), and the error probability for the Gaussian approximation as given by (10). From these figures we see that the upper bound (8) approaches the exact error probability as given by the Webb simulation as P_e becomes small. In Fig. 1, the Gaussian approximation consistently overbounds the simulation error probability, whereas in Fig. 2, the Gaussian curve first underbounds the Webb curve for lower $\bar{n}_s$ and then crosses over and overbounds the Webb curve as $\bar{n}_s$ increases. The cross-over points occur at increasing values of signal photon level as the background photon level increases.

4 Turbo-Coded M-ary PPM

4.1 Turbo Encoder

A rate 1/3 turbo encoder is shown in Fig. 3. It consists of two rate 1/2 constituent codes and an interleaver of length N. The input $\mathbf{u} = (u_1, \ldots, u_N)$ is a block of independent, uniformly distributed information bits. We use the trellis termination method in [6], which takes m additional steps to return the encoders to the all zeroes state.

In this paper, the constituent codes shall be rate 1/2, recursive, systematic convolutional codes. The three outputs of the rate $1/3$ turbo encoder include the systematic bit x_0, and the two parity bits x_{1p} and x_{2p}. The permuted systematic bit from the second convolutional code is not transmitted across the channel. Thus, a total of $n = 3(N+m)$ bits are transmitted for the rate 1/3 code. The bits are grouped into M-ary PPM symbols. For concreteness, in this paper $M = 256$.

4.2 Turbo Decoder

We use a turbo decoder structure and notation as in [2], shown in Fig. 4. Although this structure was designed as a turbo decoder for a binary AWGN channel, part of its beauty is that each soft-input soft-output (SISO) module need not know anything about the channel in order to operate— its computation is determined completely by the a priori distribution $P(\mathbf{c}; I)$ and knowledge of the code structure. Thus, given the a priori probability distributions, the turbo decoder operates in the usual way. Details are contained in [1–3, 6].

To properly initialize the turbo decoder, we must determine the a priori probability of codewords for each constituent code.[1] Let $\mathbf{c} = (c_0, c_1)$ denote a possible constituent code codeword. As in [2], we define $P(\mathbf{c}; I) = \{P_k(\mathbf{c}; I)\}$, for $k = 1, \ldots, N+m$, where for SISO 1

$$P_k(\mathbf{c}; I) = \Pr[\text{codeword } (x_0, x_{1p}) \text{ is } \mathbf{c} \text{ at time } k | \text{ all soft counts from all symbols}], \tag{11}$$

and for SISO 2

$$P_k(\mathbf{c}; I) = \Pr[\text{codeword } (\pi(x_0), x_{2p}) \text{ is } \mathbf{c} \text{ at time } k | \text{ all soft counts from all symbols}]. \tag{12}$$

Note that all soft counts in the conditioning in Equations (11) and (12) are irrelevant to computing $P_k(\mathbf{c}; I)$ except those from PPM symbols that contain the kth constituent codeword bits.

[1] By "a priori" probability, we mean that there is conditioning on the the receiver decision statistics, but no conditioning on the turbo code structure, i.e., for the purposes of computing $P(\mathbf{c}; I)$, the components of $\mathbf{c}$ are assumed to be independent and uniformly distributed. This the usual meaning in the the context of turbo codes; in other contexts, conditioning on receiver statistics would be termed a posteriori.

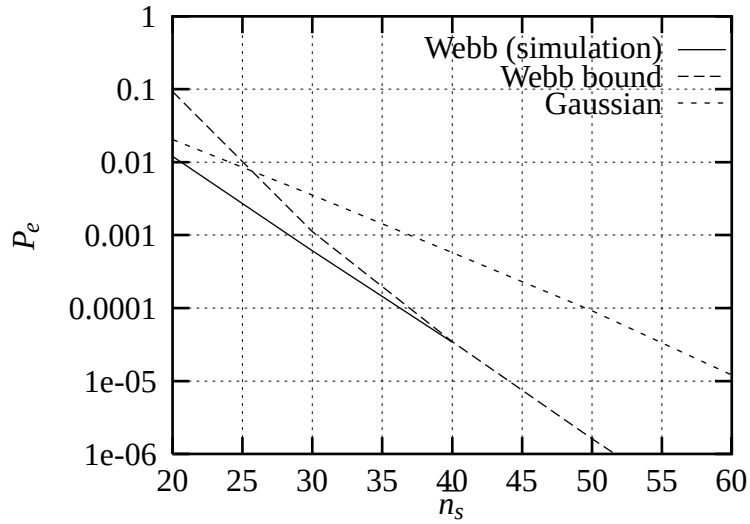

Figure 1: Comparison of error probabilities using Webb and Gaussian models, $\bar{n}_b = 0.01$, optimized gain.

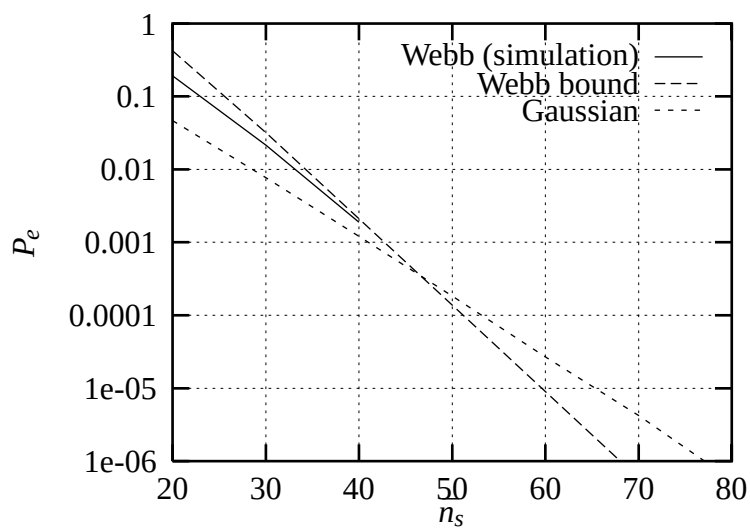

Figure 2: Comparison of error probabilities using Webb and Gaussian models, $\bar{n}_b = 1$, optimized gain.

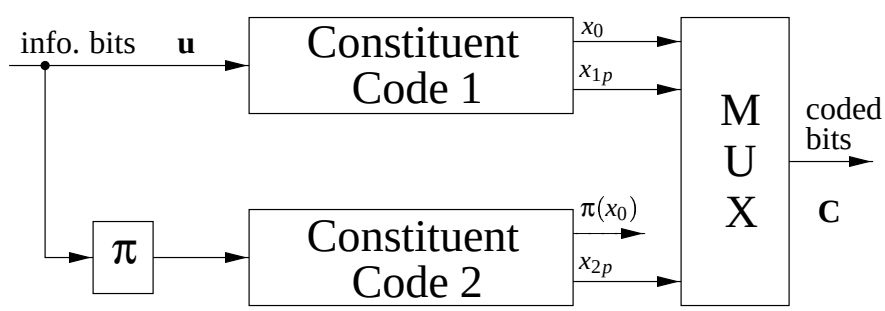

Figure 3: Rate 1/3 Turbo Encoder.

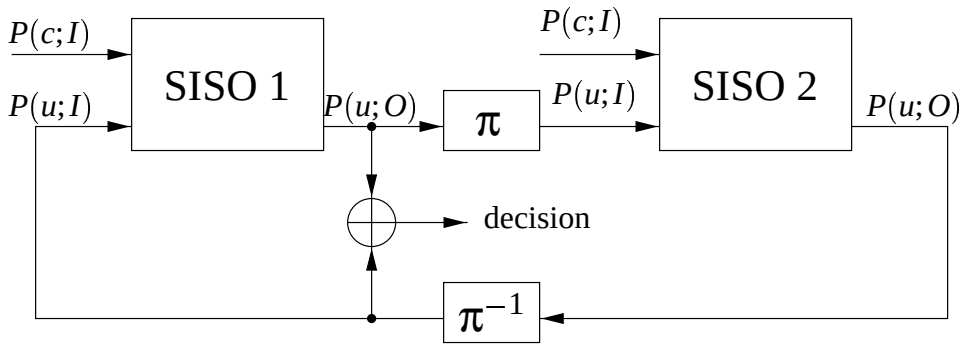

Figure 4: Turbo decoder.

That is, a soft count does not give information about (x_0, x_{1p}) unless it is a soft count from a PPM symbol that depends on x_0 or x_{1p}.

To compute $P_k(\mathbf{c}; I)$, there are two cases to consider. We consider SISO 1 here; the analysis is identical for SISO 2, except that (x_o, x_{1p}) is replaced by $(\pi(x_0), x_{2p})$.

Case 1: *The bits (x_0, x_{1p}) which form the kth constituent codeword are grouped into two separate PPM symbol epochs s and t.*
In this case, let x_0 be the lth bit of the sth PPM symbol, let x_{1p} be the mth bit of the tth PPM symbol, and let $\mathbf{y} = (y_0, \ldots, y_{255})$ and $\mathbf{z} = (z_0, \ldots, z_{255})$ denote the two sets of soft counts from the two transmitted PPM symbols. Then

$$\begin{aligned} P_k(\mathbf{c}; I) &= P_k((c_0, c_1); I) \\ &= P(\text{bit } l \text{ of } s\text{th PPM symbol is } c_0 | \mathbf{y}) && (13) \\ &\quad \cdot P(\text{bit } m \text{ of } t\text{th PPM symbol is } c_1 | \mathbf{z}) && (14) \\ &= \left(\sum_{\substack{\mathbf{a}=(a_1,\ldots,a_8) \\ a_l = c_0}} P(\mathbf{a}|\mathbf{y}) \right) \cdot \left(\sum_{\substack{\mathbf{a}=(a_1,\ldots,a_8) \\ a_m = c_1}} P(\mathbf{a}|\mathbf{z}) \right), && (15) \end{aligned}$$

where Equation (14) follows by the independence of the soft counts from one PPM symbol to the next, and where in Equation (15) $\mathbf{a}$ is the 8-bit vector defining a 256-PPM symbol.

Case 2: *The bits (x_0, x_{1p}) which form the kth constituent codeword are grouped into the same PPM symbol epoch s.*
In this case, let x_0 be the lth bit of the sth PPM symbol, let x_{1p} be the mth bit of the sth PPM symbol, and let $\mathbf{y} = (y_0, \ldots, y_{255})$ denote the set of soft counts from the sth PPM symbol. Then

$$\begin{aligned} P_k(\mathbf{c}; I) &= P_k((c_0, c_1); I) \\ &= P(\text{bit } l \text{ and } m \text{ of } s\text{th PPM symbol is } c_0 \text{ and } c_1\text{, resp.} | \mathbf{y}) \\ &= \sum_{\substack{\mathbf{a}=(a_1,\ldots,a_8) \\ a_l = c_0 \\ a_m = c_1}} P(\mathbf{a}|\mathbf{y}). && (16) \end{aligned}$$

In either Case 1 or Case 2, we need to compute the probability that a given 256-PPM symbol $\mathbf{a} = (a_1, \ldots, a_8)$ was transmitted, given its corresponding set of 256 soft counts $\mathbf{y} =$

$(y_0, \ldots, y_{255})$. Although we must omit the details, it can be shown by standard usage of Bayes rule, independence of the slot statistics, and a priori equiprobability of each slot containing a pulse, that

$$P(\mathbf{a}|\mathbf{y}) = \frac{L_{\mathbf{a}}}{\sum_{i=0}^{255} L_i}, \tag{17}$$

where we use **a** as both a PPM symbol and an index to a slot, and where L_i is the likelihood ratio of the ith slot containing a signal pulse given the soft count in that slot, i.e., the ratio of Equation (4) with $\bar{n} = \bar{n}_b + \bar{n}_s$ to Equation (4) with $\bar{n} = \bar{n}_b$. Equation (17) may be used in Equations (15) and (16) to compute the a priori probabilities needed for the SISO modules.

5 Performance Simulations

Using the method of the previous section, simulations were conducted for rate 1/3 turbo coded 256-PPM and a typical APD detector. The constituent codes had either 4 states and identical generators of $(5/7)_{oct}$, or 8 states and identical generators of $(17/15)_{oct}$. The interleaver had length 16382 and represented a random permutation. The signal varied from $\bar{n}_s = 20$ to 30 photons/slot, and the background intensity was fixed at $\bar{n}_b = 10$ photons/slot. We used the same APD parameters as in Section 3, except that the gain was fixed at 80, and we used the shot noise limited case, i.e., we assumed negligible additive thermal noise in the APD. The turbo decoder performed 10 iterations before bit decisions were made. The simulations were continued until 100 error-containing blocks were processed. This typically involved the simulation of 10,000 or more bit errors.

Reed-Solomon performance was determined by simulating the soft counts using a program to generate Webb deviates, computing the resulting PPM symbol error rate (SER) when the maximum likelihood rule is used [12], and using a formula for the performance of Reed-Solomon code based on that SER. Erasures were not considered.

Fig. 5 shows the performance of rate 1/3 coded 256-PPM as a function of input SER. (Fig. 6 shows the same simulation data, as a function of $\bar{n}_s$.) Since the turbo decoder does not make an explicit determination of PPM symbols, the input SER is technically not defined for turbo codes; the SER used in the plot is that which would have occurred had the maximum likelihood rule been used to make PPM symbol decisions. The three curves for turbo codes represent the 4-state noninterleaved PPM, 4 state interleaved PPM, and 8 state interleaved PPM simulations. By noninterleaved PPM, we mean that the bits at the output of the turbo encoder are grouped into 8-bit blocks directly and PPM modulated. This order is $(x_0, x_{1p}, x_{2p}, x_0, x_{1p}, x_{2p}, \ldots, x_0, x_{1p}, x_{2p})$. For the interleaved PPM, the order of the bits has been partially randomized before grouping into PPM symbols. The effect of the interleaver before the modulator is to spread out related bits into different PPM symbols.

Acknowledgements: The authors acknowledge Dariush Divsalar and Victor Vilnrotter for helpful discussions about turbo codes and the APD detector.

References

[1] L. R. Bahl, J. Cocke, F. Jelinek, and J. Raviv. Optimal decoding of linear codes for minimizing symbol error rate. *IEEE Trans. Inform. Theory*, IT-20:284–287, March 1974.

[2] S. Benedetto, D. Divsalar, G. Montorsi, and F. Pollara. A soft-input soft-output maximum a posteriori (MAP) module to decode parallel and serial concatenated codes. *The*

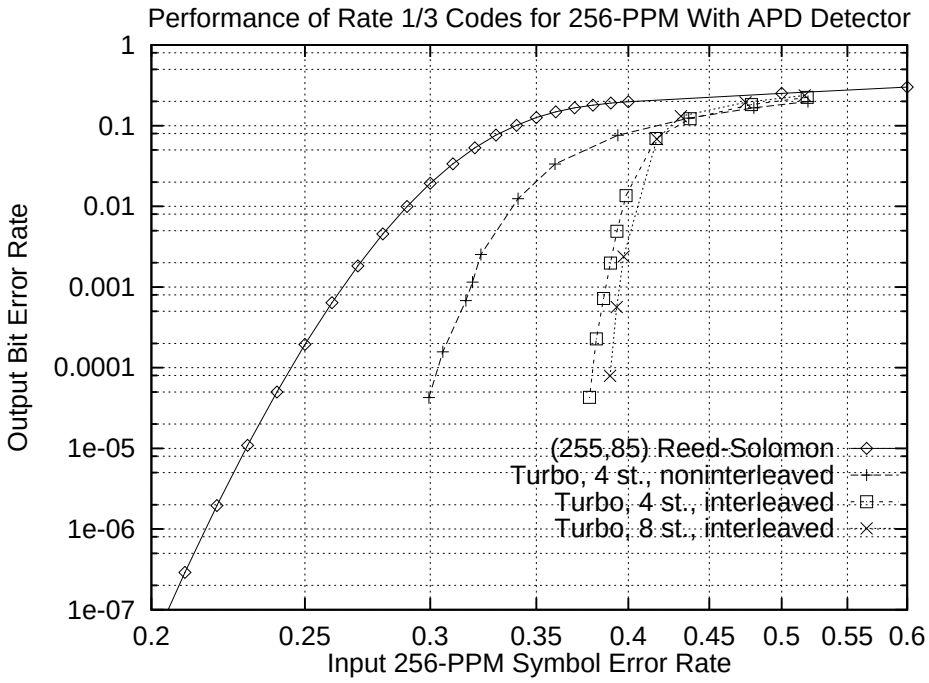

Figure 5: Performance of rate 1/3 codes as a function of input SER.

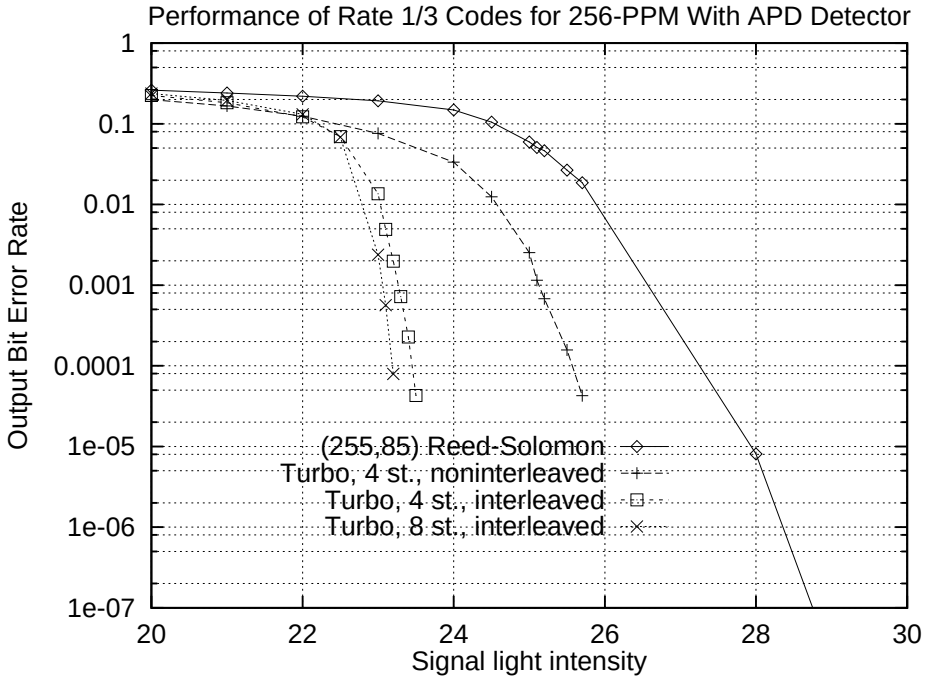

Figure 6: Performance of rate 1/3 codes as a function of signal intensity.

Telecommunications and Data Acquisition Progress Report, 42(127):1–20, November 1996.

[3] Claude Berrou, Alain Glavieux, and Punya Thitimajshima. Near Shannon limit error-correcting coding and decoding: turbo-codes. In *Proc., IEEE Int. Conf. on Communications*, pages 1064–1070, May 1993.

[4] J. Conradi. The distribution of gains in uniformly multiplying avalanche photodiodes: Experimental. *IEEE Transactions on Electron Devices*, ED-19(6):713–718, June 1972.

[5] F. M. Davidson and X. Sun. Gaussian approximation versus nearly exact performance analysis of optical communications systems with PPM signaling and APD receivers. *IEEE Transactions on Communications*, 36(11):1185–1192, November 1988.

[6] D. Divsalar and F. Pollara. Turbo codes for deep-space communications. *The Telecommunications and Data Acquisition Progress Report*, 42(120):29–39, February 1995.

[7] L. Hughes. A simple upper bound on the error probability for orthogonal signals in white noise. *IEEE Transactions on Communications*, COM-40(4):670, April 1992.

[8] R. J. McIntyre. The distribution of gains in uniformly multiplying avalanche photodiodes: Theory. *IEEE Transactions on Electron Devices*, ED-19(6):703–713, June 1972.

[9] George Stephen Mecherle. *Maximized data rate capability for optical communication using semiconductor devices with pulse position modulation*. PhD thesis, University of Southern California, May 1986.

[10] W. H. Press, W. T. Vetterling, S. A. Teukolsky, and B. P. Flannery. *Numerical Recipes in C*. Cambridge University Press, New York, 1992.

[11] J. K. Townsend and K. S. Shanmugan. On improving the computational efficiency of digital lightwave link simulation. *IEEE Transactions on Communications*, 38(11), November 1990.

[12] V. Vilnrotter, M. Simon, and M. Srinivasan. Maximum likelihood detection of PPM signals governed by an arbitrary point process plus additive gaussian noise. JPL Publication 98-7, April 1998.

[13] P. P. Webb, R. J. McIntyre, and J. Conradi. Properties of avalanche photodiodes. *RCA Review*, 35:234–278, June 1974.